IEEE Access
Multidisciplinary | Rapid Review | Open Access Journal

Received June 7, 2021, accepted June 18, 2021, date of publication June 21, 2021, date of current version June 29, 2021.

Digital Object Identifier 10.1109/ACCESS.2021.3091210

An Improved Three-Stages Cascading Passivity-Based Control of Grid-Connected LCL Converter in Unbalanced Weak Grid Condition

JIANGUO LI[1], (Member, IEEE), YAJING ZHANG[1], (Member, IEEE), YUMING ZHAO[2], LI REN[3], JIUHE WANG[1], AND YUFAN LIU[1]

[1]School of Automation, Beijing Information Science and Technology University, Beijing 100192, China
[2]Shenzhen Power Supply Corporation, Shenzhen 518048, China
[3]Tianjin Research Institute for Advanced Equipment, Tsinghua University, Tianjin 300300, China

Corresponding author: Jianguo Li (lijianguo@bistu.edu.cn)

This work was supported in part by the Beijing Natural Science Foundation under Grant 3202010 and Grant 3204040, and in part by Beijing Information Science and Technology University, Scientific Research Promotion Project, under Grant 2020KYNH209.

ABSTRACT This paper proposes an improved three-stages cascading passivity-based control (PBC) for a grid -connected LCL converter in unbalanced weak grid condition. In general, the traditional double-loop control based on positive and negative sequence transformations is used in grid-connected converter control in unbalanced weak grid condition. However, it is time consuming for second harmonic filtering, and positive and negative sequence currents need to be controlled separately. The PBC has strong robustness to interference, and the line voltage based PBC can deal with the voltage unbalance effectively and easily without negative sequence transformation. But the traditional PBC needs six variables and three damping coefficients for the grid-connected LCL converter in unbalanced grid condition, and it has the disadvantage of difficult implementation. The improved PBC can realize the same control effect with three-stages cascading PBCs of two variables and one damping coefficient, and it has the advantages of easy implementation, good performance and high stability. First, the modeling and controller design are detailed described. Then the SIMULINK simulation results demonstrate the benefits of the improved control strategy. Finally, a grid-connected LCL converter prototype of 5kW is built and the experimental results verify the correctness and effectivity of the improved three-stages PBC strategy.

INDEX TERMS Improved passivity-based control, LCL converter, unbalanced weak grid.

I. INTRODUCTION

A grid-connected converter is a connector between AC power grid and DC power supply or DC load. Thus, it plays a significant role of power injection from distributed energy source to AC grid, such as PV and wind power energy source [1], [2]. However, compared with traditional energy source, the grid-connected converter's voltages, which are based on pulse width modulation (PWM), are pulse waves with multiple harmonics, and some measures must be taken to reduce and even eliminate these harmonics [3], [4].

A low-pass passive filter is normally used to eliminate harmonics and improve power quality of the grid-connected converter. Compared with a L-type filter, a LCL-type filter has the advantages of smaller inductor, lower cost and higher harmonic elimination rate, but a LCL-type filter also has the risk of resonance, especially in weak grid condition [5], [6].

A weak grid does widely exist, especially in remote micro-grid formed by distributed energy source. Particularly, there are usually long distant transmission line and multi-stages transformers between the micro-grid and the power grid. As a result, the grid often suffers from high grid impedance and low short circuit capacity, and these form the characteristics of weak grid [7]. In addition, there also has high probability of unbalance voltages, because of high grid impedance and three-phases unbalance loads or single-phase loads [8].

In a weak grid, the point of common coupling (PCC) voltages have nonnegligible impedance and unbalance voltages with multiple harmonics. Furthermore the 'polluted' voltages and internal impedance influence the grid-connected LCL converter's operation, cause resonance, and even destroy its stability [9], [10]. Thus, some measures must be taken to deal

The associate editor coordinating the review of this manuscript and approving it for publication was Shuaihu Li.

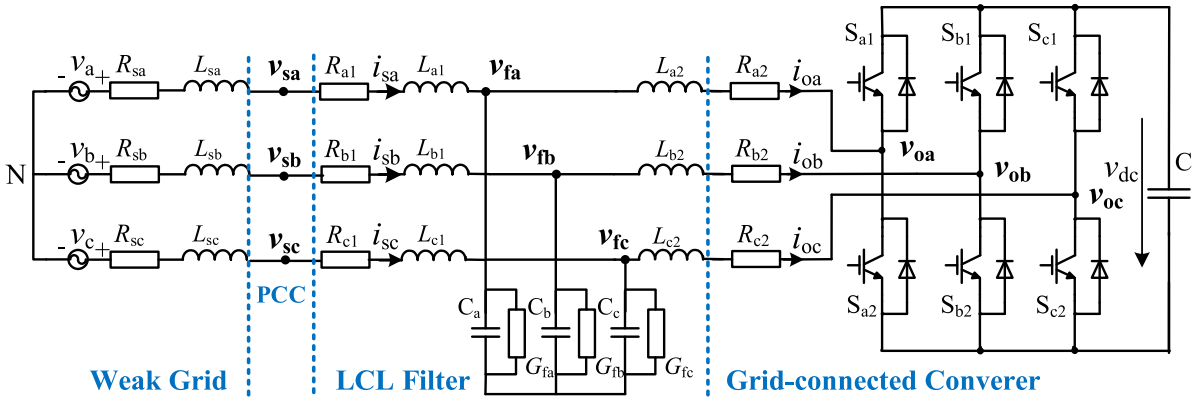

FIGURE 1. Equivalent topology of the grid-connected LCL converter in weak grid.

with the possible resonance and instability of the grid-connect LCL converter in unbalanced weak grid.

To avoid LCL filter resonance, passive damping (PD) and active damping (AD) are often used. The PD is easily applied with a paralleled or a series connected damping resistor to damp the resonant frequency, but it increases power loss and decreases power efficiency. Compared with PD, AD is lossless and costless. However, AD needs capacitor currents or capacitor voltages feedback. The capacitor currents-based AD needs high-precision current sensor and controller, the capacitor voltages-based AD needs high bandwidth switching devices and digital differentiator, which often results in amplifies noises [11], [12].

In the grid-connected converter studies, the linear control strategies, which includes PI control, PR control, and so on, are early used. However, the linear converter cannot achieve accurate control, and it is also difficult to achieve global stable control. So more and more nonlinear control strategies are applied to the grid-connected converter, such as the predictive control (PRC) [13]. Obviously, nonlinear control strategy is one of the most promising techniques to reduce or even remove the oscillation, and to achieve the high robustness of the system. However, nonlinear control strategies are mostly difficult to realize the real time control with complex modelling and a large amount of computation.

In the weak grid studies, a robust current control is used to improve the converter's stability [14], a grid impedance estimation based adaptive control is used to maintain the converter's stable operation in [15], a quasi-proportional resonance feedforward control is used to enhance the converter's robust ability [16], a small-signal disturbance compensation control is used to mitigate the weak grid's influence [17], a novel grid voltage feedforward control is used to suppress the effect of grid voltage harmonics [18], all these studies greatly improve the performance of the converter in weak grid. However, the studies are mainly based on traditional nonlinear control, some complex models are needed, and a large amount of computation are also needed in practical application. In view of these studies, a valid nonlinear control strategy, which has fewer parameters, simple design, easy application and good performance, should be conducted to improve the grid connected LCL converter's performance in unbalanced weak grid condition.

The passivity-based control (PBC), which was proposed by R. Ortega and M. Spong in 1989, can be stable globally in nonlinear system and has the advantages of simple design and easy implementation [19], [20], and it has been used in power conversion system [21], rectifier [22], [23], PV [20], [24], STATCOM [25] and other grid-connected LCL converter [26], [27]. Obviously, all these studies promote electrical applications of PBC. However, there are often many state variables and damping parameters in traditional PBC, and it is difficult to adjust these parameters in practical application.

The major contribution of this paper is to propose an improved three-stages cascading PBC, a traditional PBC with six-variables is decomposed to three cascading PBCs with two-variables, and each PBC has only one parameter, which makes it easy to use in practical application.

This paper is organized as follows. In Section II, the equivalent topology is introduced and analysed thoroughly. In Section III, the mathematical models based on Euler-Lagrange (EL) equations are proposed. In Section IV, the improved three-stages cascading PBC controller is designed. Later in Section V and VI, the simulation and prototype experiment results are given separately. Finally, a conclusion is given in Section VII.

II. EQUIVALENT TOPOLOGY ANALYSIS

Fig. 1 shows equivalent topology of a grid-connected LCL converter in weak grid condition. The converter is made up of three parts: The part I is a three-phases two-levels converter, and R_{a2}, R_{b2} and R_{c2} are used to simulate its conducting and switching losses, and the currents and voltages are i_{oa}, i_{ob}, i_{oc}, v_{oa}, v_{ob} and v_{oc}, respectively. The part II is a LCL-type low-pass filter. R_{a1}, R_{b1} and R_{c1} are used to simulate the series losses related with currents, and G_{fa}, G_{fb} and G_{fc} are used to simulate the paralle1 losses related with voltages, and the LCL filter voltages are v_{fa}, v_{fb} and v_{fc}, respectively. The part III is a weak grid source. R_{sa}, R_{sb}, R_{sc}, L_{sa}, L_{sb} and

L_{sc} are used to simulate the internal resistors and inductors, respectively. v_a, v_b and v_c are the power source voltages, and v_{sa}, v_{sb} and v_{sc} are PCC voltages.

According to Kirchhoff voltage law (KVL) and Kirchhoff current law (KCL), the converter voltages and currents differential equations can be expressed as follow,

$$\begin{cases} (L_{si}+L_{i1})\dfrac{\mathrm{d}i_{si}}{\mathrm{d}t}+(R_{si}+R_{i1})i_{si}+v_{fi}=v_i, & i=\text{a,b,c} \\ L_{i2}\dfrac{\mathrm{d}i_{oi}}{\mathrm{d}t}+R_{i2}i_{oi}-v_{fi}=-v_{oi}, & i=\text{a,b,c} \\ C_i\dfrac{\mathrm{d}v_{fi}}{\mathrm{d}t}-i_{si}+i_{oi}+G_{fi}v_{fi}=0, & i=\text{a,b,c} \end{cases} \tag{1}$$

where i_{si} and i_{oi} are grid currents and converter currents, v_{fi} are filter voltages, v_i are power source voltages, and v_{oi} are converter voltages, respectively.

III. MATHEMATICAL MODEL OF GRID-CONNECTED LCL CONVERTER

A. MODEL IN ABC COORDINATES

Considering that a three-phases three-lines converter meets $i_{sa}+i_{sb}+i_{sc}=0$ and $i_{oa}+i_{ob}+i_{oc}=0$ all the time, it can be derived that,

$$\begin{cases} L_{s1}\dfrac{\mathrm{d}i_{sa}}{\mathrm{d}t}+R_{s1}i_{sa}+\dfrac{v_{fab}-v_{fca}}{3}=\dfrac{v_{ab}-v_{ca}}{3} \\ L_{s1}\dfrac{\mathrm{d}i_{sb}}{\mathrm{d}t}+R_{s1}i_{sb}+\dfrac{v_{fbc}-v_{fab}}{3}=\dfrac{v_{bc}-v_{ab}}{3} \\ L_{s1}\dfrac{\mathrm{d}i_{sc}}{\mathrm{d}t}+R_{s1}i_{sc}+\dfrac{v_{fca}-v_{fbc}}{3}=\dfrac{v_{ca}-v_{bc}}{3}, \end{cases} \tag{2}$$

$$\begin{cases} L_2\dfrac{\mathrm{d}i_{oa}}{\mathrm{d}t}+R_2i_{oa}-\dfrac{v_{fab}-v_{fca}}{3}=-\dfrac{v_{oab}-v_{oca}}{3} \\ L_2\dfrac{\mathrm{d}i_{ob}}{\mathrm{d}t}+R_2i_{ob}-\dfrac{v_{fbc}-v_{fab}}{3}=-\dfrac{v_{obc}-v_{oab}}{3} \\ L_2\dfrac{\mathrm{d}i_{oc}}{\mathrm{d}t}+R_2i_{oc}-\dfrac{v_{fca}-v_{fbc}}{3}=-\dfrac{v_{oca}-v_{obc}}{3}, \end{cases} \tag{3}$$

$$\begin{cases} C\dfrac{\mathrm{d}v_{fab}}{\mathrm{d}t}-i_{sa}+i_{sb}+i_{oa}-i_{ob}+G_fv_{fab}=0 \\ C\dfrac{\mathrm{d}v_{fbc}}{\mathrm{d}t}-i_{sb}+i_{sc}+i_{ob}-i_{oc}+G_fv_{fbc}=0 \\ C\dfrac{\mathrm{d}v_{fca}}{\mathrm{d}t}-i_{sc}+i_{sa}+i_{oc}-i_{oa}+G_fv_{fca}=0, \end{cases} \tag{4}$$

where $L_{s1}=L_s+L_1$, $R_{s1}=R_s+R_1$, v_{ab}, v_{bc}, v_{ca}, v_{fab}, v_{fbc}, v_{fca} v_{oab}, v_{obc} and v_{oca} are line voltages of power source, LCL filter and converter, respectively.

B. MODEL IN DQ COORDINATES

The synchronous rotation coordinate is adopted, and the dq voltages and currents are shown as

$$\begin{pmatrix} i_{sd} \\ i_{sq} \end{pmatrix}=\boldsymbol{T}_1\begin{pmatrix} i_{sa} \\ i_{sb} \\ i_{sc} \end{pmatrix},\begin{pmatrix} i_{od} \\ i_{oq} \end{pmatrix}=\boldsymbol{T}_1\begin{pmatrix} i_{oa} \\ i_{ob} \\ i_{oc} \end{pmatrix}, \tag{5}$$

$$\begin{pmatrix} v_d \\ v_q \end{pmatrix}=\boldsymbol{T}_2\begin{pmatrix} v_{ab} \\ v_{bc} \\ v_{ca} \end{pmatrix},$$

$$\begin{pmatrix} v_{fd} \\ v_{fq} \end{pmatrix}=\boldsymbol{T}_2\begin{pmatrix} v_{fab} \\ v_{fbc} \\ v_{fca} \end{pmatrix},\begin{pmatrix} v_{od} \\ v_{oq} \end{pmatrix}=\boldsymbol{T}_2\begin{pmatrix} v_{oab} \\ v_{obc} \\ v_{oca} \end{pmatrix}, \tag{6}$$

where i_{sd}, i_{sq}, i_{od} and i_{oq} are dq coordinate currents, v_d, v_q, v_{od}, v_{oq}, v_{fd} and v_{fq} are dq coordinate voltages, $\boldsymbol{T}_1$ and $\boldsymbol{T}_2$ are transform matrices from abc coordinate to dq coordinate as

$$\boldsymbol{T}_1=\frac{2}{3}\begin{pmatrix} \cos(\omega t) & \cos(\omega t-2\pi/3) & \cos(\omega t+2\pi/3) \\ -\sin(\omega t) & -\sin(\omega t-2\pi/3) & -\sin(\omega t+2\pi/3) \end{pmatrix}, \tag{7}$$

$$\boldsymbol{T}_2=\frac{2}{3}\begin{pmatrix} \cos(\omega t+\pi/6) & \cos(\omega t-\pi/2) & \cos(\omega t+5\pi/6) \\ -\sin(\omega t+\pi/6) & -\sin(\omega t-\pi/2) & -\sin(\omega t+5\pi/6) \end{pmatrix}. \tag{8}$$

Thus, the equation (2)-(4) can be expressed as

$$\begin{cases} L_{s1}\dfrac{\mathrm{d}i_{sd}}{\mathrm{d}t}+R_{s1}i_{sd}-\omega L_{s1}i_{sq}+\dfrac{v_{fd}}{\sqrt{3}}=\dfrac{v_d}{\sqrt{3}} \\ L_{s1}\dfrac{\mathrm{d}i_{sq}}{\mathrm{d}t}+\omega L_{s1}i_{sd}+R_{s1}i_{sq}+\dfrac{v_{fq}}{\sqrt{3}}=\dfrac{v_q}{\sqrt{3}}, \end{cases} \tag{9}$$

$$\begin{cases} L_2\dfrac{\mathrm{d}i_{od}}{\mathrm{d}t}+R_2i_{od}-\omega L_2i_{oq}-\dfrac{v_{fd}}{\sqrt{3}}=-\dfrac{v_{od}}{\sqrt{3}} \\ L_2\dfrac{\mathrm{d}i_{oq}}{\mathrm{d}t}+\omega L_2i_{od}+R_2i_{oq}-\dfrac{v_{fq}}{\sqrt{3}}=-\dfrac{v_{oq}}{\sqrt{3}}, \end{cases} \tag{10}$$

$$\begin{cases} L_{s1}\dfrac{\mathrm{d}i_{sd}}{\mathrm{d}t}+R_{s1}i_{sd}-\omega L_{s1}i_{sq}+\dfrac{v_{fd}}{\sqrt{3}}=\dfrac{v_d}{\sqrt{3}} \\ \dfrac{C_f}{3}\dfrac{\mathrm{d}v_{fd}}{\mathrm{d}t}-\dfrac{i_{sd}}{\sqrt{3}}+\dfrac{i_{od}}{\sqrt{3}}+\dfrac{G_f}{3}v_{fd}-\dfrac{\omega C_f}{3}v_{fq}=0 \\ \dfrac{C_f}{3}\dfrac{\mathrm{d}v_{fq}}{\mathrm{d}t}-\dfrac{i_{sq}}{\sqrt{3}}+\dfrac{i_{oq}}{\sqrt{3}}+\dfrac{\omega C_f}{3}v_{fd}+\dfrac{G_f}{3}v_{fq}=0. \end{cases} \tag{11}$$

Then, the mathematical model of the weak grid-connected LCL converter in EL form is naturally achieved.

$$\boldsymbol{M}\dot{\boldsymbol{X}}+\boldsymbol{J}\boldsymbol{X}+\boldsymbol{R}\boldsymbol{X}=\boldsymbol{V}, \tag{12}$$

where $\boldsymbol{M}$ is a positive definite symmetric coefficient matrix, that is $\boldsymbol{M}^{\mathrm{T}}=\boldsymbol{M}$. $\boldsymbol{J}$ is an anti-symmetric coefficient matrix, that is $\boldsymbol{J}^{\mathrm{T}}=-\boldsymbol{J}$. $\boldsymbol{R}$ is a positive coefficient matrix, that is $\boldsymbol{R}^{\mathrm{T}}=\boldsymbol{R}$. And it satisfies $\boldsymbol{R}>0$, which means that the converter has dissipative character. $\boldsymbol{X}$ is the state vector, and $\boldsymbol{V}$ is the input vector.

$$\boldsymbol{J}=\begin{pmatrix} 0 & -\omega L_{s1} & 0 & 0 & 1/\sqrt{3} & 0 \\ \omega L_{s1} & 0 & 0 & 0 & 0 & 1/\sqrt{3} \\ 0 & 0 & 0 & -\omega L_2 & -1/\sqrt{3} & 0 \\ 0 & 0 & \omega L_2 & 0 & 0 & -1/\sqrt{3} \\ -1/\sqrt{3} & 0 & 1/\sqrt{3} & 0 & 0 & -\omega C_f/3 \\ 0 & -1/\sqrt{3} & 0 & 1/\sqrt{3} & \omega C_f/3 & 0 \end{pmatrix}, \tag{13}$$

$$\boldsymbol{M}=\mathrm{diag}\begin{pmatrix} L_{s1} & L_{s1} & L_2 & L_2 & C_f/3 & C_f/3 \end{pmatrix}, \tag{14}$$

$$\boldsymbol{R}=\mathrm{diag}\begin{pmatrix} R_{s1} & R_{s1} & R_2 & R_2 & G_f/3 & G_f/3 \end{pmatrix}, \tag{15}$$

$$\boldsymbol{X}=\begin{pmatrix} i_{sd} & i_{sq} & i_{od} & i_{oq} & v_{fd} & v_{fq} \end{pmatrix}^{\mathrm{T}}, \tag{16}$$

$$\boldsymbol{V}=1/\sqrt{3}\begin{pmatrix} v_d & v_q & -v_{od} & -v_{oq} & 0 & 0 \end{pmatrix}^{\mathrm{T}}. \tag{17}$$

C. PASSIVITY OF LCL CONVERTER

It is assumed that the storage energy function is

$$\boldsymbol{H} = \frac{1}{2}\boldsymbol{X}^{\mathrm{T}}\boldsymbol{M}\boldsymbol{X} = \frac{1}{2}(L_{\mathrm{s}1}i_{\mathrm{sd}}^2 + L_{\mathrm{s}1}i_{\mathrm{sq}}^2 + L_2 i_{\mathrm{od}}^2 + L_2 i_{\mathrm{oq}}^2 + \frac{C_{\mathrm{f}}}{3}v_{\mathrm{fd}}^2 + \frac{C_{\mathrm{f}}}{3}v_{\mathrm{fq}}^2) \geq 0. \quad (18)$$

Therefore, the following equations can be derived as

$$\begin{aligned}\dot{\boldsymbol{H}} &= \boldsymbol{X}^{\mathrm{T}}\boldsymbol{M}\dot{\boldsymbol{X}} = \boldsymbol{X}^{\mathrm{T}}(\boldsymbol{V} - \boldsymbol{J}\boldsymbol{X} - \boldsymbol{R}\boldsymbol{X}) \\ &= \boldsymbol{X}^{\mathrm{T}}\boldsymbol{V} - \boldsymbol{X}^{\mathrm{T}}\boldsymbol{R}\boldsymbol{X} = \boldsymbol{X}^{\mathrm{T}}\boldsymbol{V} - Q(\boldsymbol{X}) \end{aligned} \quad (19)$$

It can be seen that $\boldsymbol{H}(\boldsymbol{X})$ is a positive semi-definite function and $\boldsymbol{Q}(\boldsymbol{X})$ is a positive definite function, and if the output variables $\boldsymbol{Y}$ is set as $\boldsymbol{X}$, the energy supply rate $\boldsymbol{X}^{\mathrm{T}}\boldsymbol{V}$ is valid to any input variable $\boldsymbol{V}$, that is to say that the weak grid-connected LCL converter is strictly passive according to the passivity theory.

IV. PASSIVITY BASED CONTROL OF GRID-CONNECTED LCL CONVERTER

A. TRADITIONAL PBC CONTROL

Considering that the PCC voltage is measured in the application, v_{sd}, v_{sq}, L_1 and R_1 are used instead of v_{d}, v_{q}, $L_{\mathrm{s}1}$ and $R_{\mathrm{s}1}$ in (12), where v_{sd} and v_{sq} are dq coordinate PCC voltages.

Assuming $\boldsymbol{X}^* = (i_{\mathrm{sd}}^* \; i_{\mathrm{sq}}^* i_{\mathrm{od}}^* i_{\mathrm{oq}}^* \; v_{\mathrm{fd}}^* v_{\mathrm{fq}}^*)^{\mathrm{T}}$ is the control goal, the error vector is $\boldsymbol{X}_{\mathrm{e}} = \boldsymbol{X}–\boldsymbol{X}^*$. In order to accelerate $\boldsymbol{X}$ converge to $\boldsymbol{X}^*$, a damping injecting matrix $\boldsymbol{R}_{\mathrm{d}} = \mathrm{diag}\{r_{11} \; r_{11}r_{22}r_{22}g_{33} \; g_{33}\}$ is used, where r_{11}, r_{22} and g_{33} are positive constants. And the model with state vector $\boldsymbol{X}$ can be further descripted with error vector $\boldsymbol{X}_{\mathrm{e}}$ as

$$\boldsymbol{M}\dot{\boldsymbol{X}}_{\mathrm{e}} + (\boldsymbol{R} + \boldsymbol{R}_{\mathrm{d}})\boldsymbol{X}_{\mathrm{e}} = \boldsymbol{V} - (\boldsymbol{M}\dot{\boldsymbol{X}}^* + \boldsymbol{J}\boldsymbol{X} + \boldsymbol{R}\boldsymbol{X}^* - \boldsymbol{R}_{\mathrm{d}}\boldsymbol{X}_{\mathrm{e}}). \quad (20)$$

Therefore, the traditional PBC controller can be selected as

$$\boldsymbol{V} = \boldsymbol{M}\dot{\boldsymbol{X}}^* + \boldsymbol{J}\boldsymbol{X} + \boldsymbol{R}\boldsymbol{X}^* - \boldsymbol{R}_{\mathrm{d}}\boldsymbol{X}_{\mathrm{e}}. \quad (21)$$

The traditional PBC control has six state variables, six input variables and three damping parameters, and it is often difficult to adjust these parameters in practical application.

B. IMPROVED PBC CONTROL

To simplify the traditional PBC control, it can be further decomposed to three-stages cascading PBCs by selecting appropriate state variables and input variables. According to (12), we can get three mathematical models in EL form as

$$\boldsymbol{M}_k\dot{\boldsymbol{X}}_k + \boldsymbol{J}_k\boldsymbol{X}_k + \boldsymbol{R}_k\boldsymbol{X}_k = \boldsymbol{V}_k, \quad k = 1,2,3, \quad (22)$$

where

$$\begin{cases} \boldsymbol{M}_1 = L_1\begin{pmatrix}1 & 0\\ 0 & 1\end{pmatrix}, \boldsymbol{J}_1 = \omega L_1\begin{pmatrix}0 & -1\\ 1 & 0\end{pmatrix}, \\ \boldsymbol{R}_1 = R_1\begin{pmatrix}1 & 0\\ 0 & 1\end{pmatrix}, \\ \boldsymbol{X}_1 = \begin{pmatrix}i_{\mathrm{sd}} \; i_{\mathrm{sq}}\end{pmatrix}^T, \boldsymbol{V}_1 = 1/\sqrt{3}\begin{pmatrix}v_{\mathrm{sd}} - v_{\mathrm{fd}} \; v_{\mathrm{sq}} - v_{\mathrm{fq}}\end{pmatrix}^{\mathrm{T}}, \end{cases} \quad (23)$$

$$\begin{cases} \boldsymbol{M}_2 = L_2\begin{pmatrix}1 & 0\\ 0 & 1\end{pmatrix}, \boldsymbol{J}_2 = \omega L_2\begin{pmatrix}0 & -1\\ 1 & 0\end{pmatrix}, \\ \boldsymbol{R}_2 = R_2\begin{pmatrix}1 & 0\\ 0 & 1\end{pmatrix}, \\ \boldsymbol{X}_2 = \begin{pmatrix}i_{\mathrm{od}} \; i_{\mathrm{oq}}\end{pmatrix}^T, \boldsymbol{V}_2 = 1/\sqrt{3}\begin{pmatrix}v_{\mathrm{fd}} - v_{\mathrm{od}} \; v_{\mathrm{fq}} - v_{\mathrm{oq}}\end{pmatrix}^{\mathrm{T}}, \end{cases} \quad (24)$$

$$\begin{cases} \boldsymbol{M}_3 = \frac{C_{\mathrm{f}}}{3}\begin{pmatrix}1 & 0\\ 0 & 1\end{pmatrix}, \boldsymbol{J}_3 = \frac{\omega C_{\mathrm{f}}}{3}\begin{pmatrix}0 & -1\\ 1 & 0\end{pmatrix}, \\ \boldsymbol{R}_3 = \frac{G_{\mathrm{f}}}{3}\begin{pmatrix}1 & 0\\ 0 & 1\end{pmatrix}, \\ \boldsymbol{X}_3 = \begin{pmatrix}v_{\mathrm{fd}} \; v_{\mathrm{fq}}\end{pmatrix}^T, \boldsymbol{V}_3 = 1/\sqrt{3}\begin{pmatrix}i_{\mathrm{sd}} - i_{\mathrm{od}} \; i_{\mathrm{sq}} - i_{\mathrm{oq}}\end{pmatrix}^{\mathrm{T}}. \end{cases} \quad (25)$$

Therefore, the improved three-stages cascading PBC controller can be selected as

$$\boldsymbol{V}_k = \boldsymbol{M}_k\dot{\boldsymbol{X}}_k^* + \boldsymbol{J}_k\boldsymbol{X}_k + \boldsymbol{R}_k\boldsymbol{X}_k^* - \boldsymbol{R}_{\mathrm{d}k}\boldsymbol{X}_{\mathrm{e}k}, \quad k = 1,2,3, \quad (26)$$

where $\boldsymbol{R}_{\mathrm{d}1} = \mathrm{diag}\{r_{11} \; r_{11}\}$, $\boldsymbol{R}_{\mathrm{d}2} = \mathrm{diag}\{r_{22}r_{22}\}$ and $\boldsymbol{R}_{\mathrm{d}3} = \mathrm{diag}\{g_{33} \; g_{33}\}$ are damping injecting matrices.

It can be seen that there are two state variables, two input variables and one damping coefficient in each PBC controller. In addition, the output of PBC1 is related to the reference of PBC3, and the output of PBC3 is related to the reference of PBC2, so these three PBC controllers are cascading connected as shown in Fig.2. At the meantime, the grid currents are only used in PBC1 controller, filter voltages are only used in PBC3 controller, converter currents are only used in PBC2 controller, and it means that the grid currents, filter voltages and converter currents are decoupled in the improved PBC control strategy.

C. STATE VECTOR REFERENCE

The grid current object is $\boldsymbol{X}_1^* = (i_{\mathrm{sd}}^*, i_{\mathrm{sq}}^*)^{\mathrm{T}}$, where i_{sd}^* can be decided by the DC voltage PI controller, that is

$$i_{\mathrm{sd}}^* = (k_{\mathrm{p}} + \frac{k_{\mathrm{i}}}{s})(v_{\mathrm{dc}}^* - v_{\mathrm{dc}}), \quad (27)$$

where k_{p} and k_{i} are proportional and integral coefficients, v_{dc}^* and v_{dc} are dc voltage reference and value, and the grid current reference i_{sq}^* can be set according to requirement. And the objects $\boldsymbol{X}_2^*$ and $\boldsymbol{X}_3^*$ can be decided as

$$\begin{cases} \boldsymbol{X}_3{}^* = \begin{pmatrix}v_{\mathrm{sd}} \; v_{\mathrm{sq}}\end{pmatrix}^{\mathrm{T}} - \sqrt{3}\boldsymbol{V}_1, \\ \boldsymbol{X}_2{}^* = \begin{pmatrix}i_{\mathrm{sd}} \quad i_{\mathrm{sq}}\end{pmatrix}^T - \sqrt{3}\boldsymbol{V}_3, \end{cases} \quad (28)$$

where $\boldsymbol{V_1}$ can be get from the PBC1 control result, and $\boldsymbol{V_3}$ can be get from the PBC3 control result.

D. CONVERTER VOLTAGES REFERENCE

According to the improved control strategy, the three-stages cascading PBC's output are v_{od} and v_{oq}, then we can further

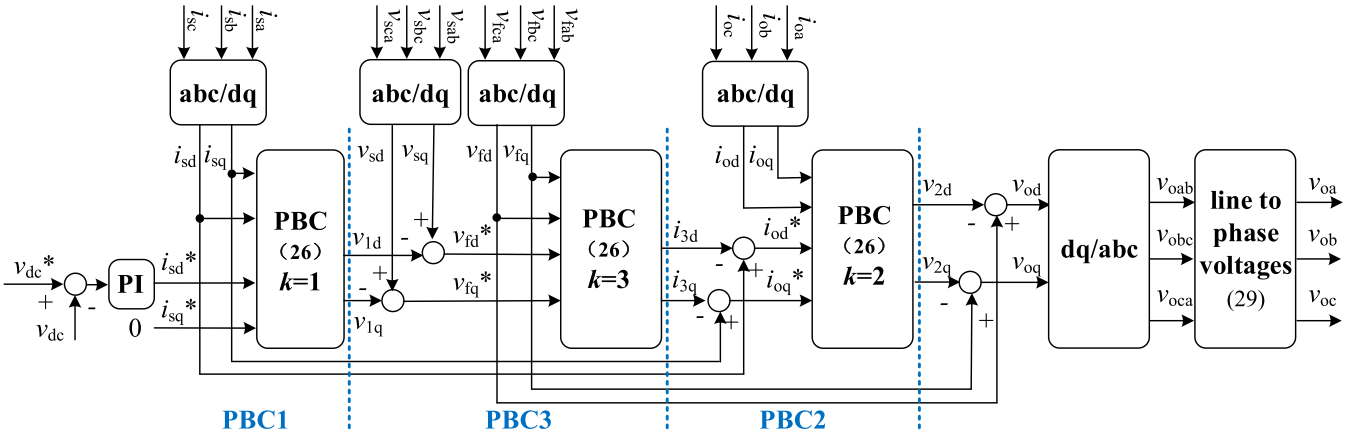

FIGURE 2. The improved three-stages PBC of the grid-connected LCL converter.

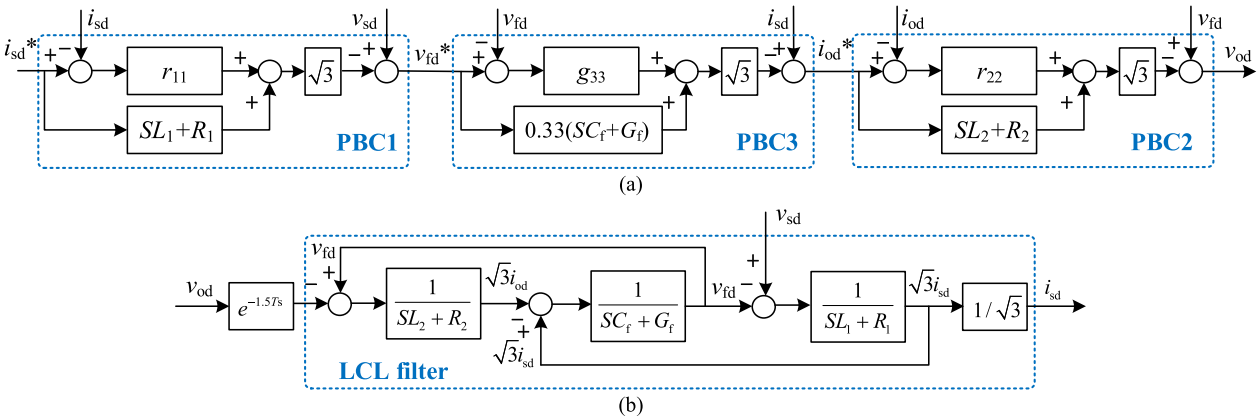

FIGURE 3. Three-stages cascading PBC control diagram of a grid connected LCL converter. (a) three-stages cascading PBC. (b) LCL filter with time delay considered.

get the converter's line and phase voltages as

$$\begin{pmatrix} v_{oab} \\ v_{obc} \\ v_{oca} \end{pmatrix} = \boldsymbol{T}_2^{-1} \begin{pmatrix} v_{od} \\ v_{oq} \end{pmatrix}, \begin{pmatrix} v_{oa} \\ v_{ob} \\ v_{oc} \end{pmatrix} = \frac{1}{3} \begin{pmatrix} 1 & 0 & -1 \\ -1 & 1 & 0 \\ 0 & -1 & 1 \end{pmatrix} \begin{pmatrix} v_{oab} \\ v_{obc} \\ v_{oca} \end{pmatrix}, \quad (29)$$

and a SPWM or SVM pulse modulation mode can be selected to generate pulses to drive switches Sa1-Sc2.

E. STABILITY ANALYSIS

The stability analysis of the improved three-stages cascading passivity-based control of grid-connected LCL converter is carried out, and the control diagram is shown in Fig.3.

The open loop transfer function of the improved PBC control LCL converter can be obtained as

$$G_{CON} = \frac{i_{sd}}{i_{sd}^*} = \frac{S^3N_3 + S_2N_2 + SN_1 + N_0}{S^4M_4 + S^3M_3 + S_2M_2 + SM_1 + M_0}, \quad (30)$$

where N_3-N_0 and M_4-M_0 are

$$\begin{aligned} N_3 &= L_1L_2C_f, \\ N_2 &= [L_1(R_2 + r_{22}) + L_2(R_1 + r_{11})]C_f + L_1L_2(G_f + 3g_{33}), \\ N_1 &= [L_1(R_2 + r_{22}) + L_2(R_1 + r_{11})](G_f + 3g_{33}) \\ &\quad +(R_1 + r_{11})(R_2 + r_{22})C_f, \\ N_0 &= (R_1 + r_{11})(R_2 + r_{22})(G_f + 3g_{33}). \quad (31) \\ M_4 &= 1.5T_sL_1L_2C_f, \\ M_3 &= 1.5T_s(L_1R_2C_f + L_2R_1C_f + L_1L_2G_f) + L_1L_2C_f, \\ M_2 &= 1.5T_s(L_1R_2G_f + L_2R_1G_f + R_1R_2C_f) \\ &\quad +(L_1R_2C_f + L_2R_1C_f + L_1L_2G_f), \\ M_1 &= 1.5T_s(R_1R_2G_f) + (L_1R_2G_f + L_2R_1G_f + R_1R_2C_f), \\ M_0 &= R_1R_2G_f. \quad (32) \end{aligned}$$

According to the open-loop transfer function shown in equation (30), the Bode diagram of the three-stages cascading PBC control strategy can be obtained in Fig.4. It shows that the phase margin and magnitude margin are 54.1° and 11.6dB, respectively, and the system is stable.

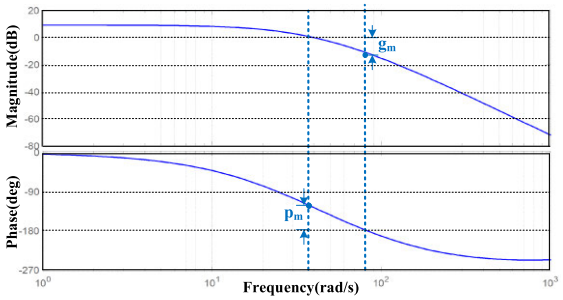

FIGURE 4. Bode diagram of open-loop system with three-stages cascading PBC.

V. SIMULATION VERIFICATION

To verify the improved three-stages cascading PBC of grid connected LCL converter in unbalanced weak grid condition, SIMULINK simulations in different weak grid conditions are carried out, the main circuit parameters are shown in Table 1, and the control coefficients are shown in Table 2.

A. STRONG GRID SIMULATION

A strong grid is simulated by the power source whose internal resistance and inductance are all zeros. In Fig.5(a), the DC voltage stays at the reference value at the first. At the time t_4, a 50Ω resistor is put in the DC capacitor, and the currents track the active current step rapidly, whose response time is less than 5ms. In Fig.5 (b), at the time t_5, t_6, t_7 and t_8, the reactive current reference is set as 20A, 0A, −20A and 20A, respectively, and the currents also track the reactive current references step rapidly, whose response time is also less than 5ms all the time. The currents' total harmonic distortion (THD) is less than 2.39% in the strong grid simulation process.

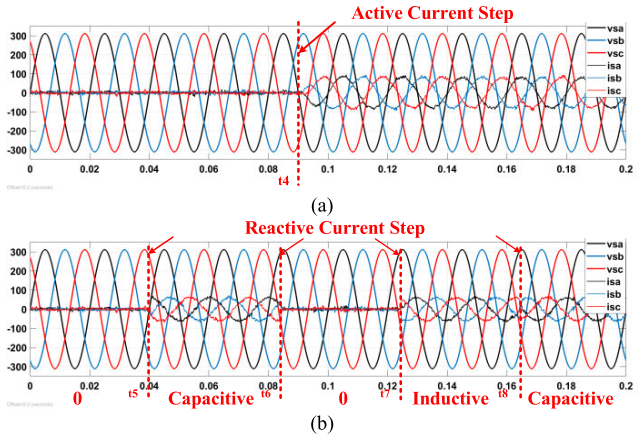

FIGURE 5. PCC voltages and currents waveforms in strong grid simulation. (a) In active current step. (b) In capacitive and inductive currents step.

B. WEAK GRID SIMULATION

In the simulation, the power source internal resistance and inductance are used to simulate weak grid. In Fig.6 (a), the power sources are perfect sinusoidal waves at the first, and the converter outputs 20A capacitive current. At the time t_9, the internal resistance and inductance are set as 0.5Ω and 10mH, respectively. The PCC voltages waves deteriorate with total harmonic distortion (THD) of 7.59%, but the currents are still sinusoidal balanced waves with same amplitudes, and the currents' THD is 3.83%. At the time t_{10}, the reference current is set as −20A inductive current, the PCC voltages decrease, however the currents track the reactive current step with same sinusoidal balanced waves and same amplitudes.

In Fig.6 (b), the power sources are perfect sinusoidal waves with 100Ω resistor load at the first. At the time t_{11}, the power source internal resistance and inductance are set as 0.5Ω and 10mH, respectively, and the PCC voltages waves deteriorate with many harmonics. However, the currents are still perfect sinusoidal balanced waves with same amplitude. At the time t_{12}, another 100Ω resistor load is put in, the currents are still perfect sinusoidal balanced waves with twice amplitude.

TABLE 1. Main circuit parasmeters of simulation.

Parameters	Value
Rated AC voltage (V)	380
Rated DC voltage (V)	750
Grid-side filter induct. L_1 (mH)	1.2
Converter-side filter induct. L_2 (mH)	4.8
Filter capacitor C (μF)	8.0
Filter series resistor R_1 (Ω)	0.1
Converter series resistor R_2 (Ω)	0.2
Filter parallel admittance G_f (1/Ω)	0.0002
DC-link capacitor (μF)	1100
Switching frequency (kHz)	12.8

TABLE 2. Control coefficients of simulation.

Coefficients	Value
DC voltage control kp	0.5
DC voltage control ki	40
Damping coefficient r_{11}	10
Damping coefficient r_{22}	150
Damping coefficient g_{33}	0.025

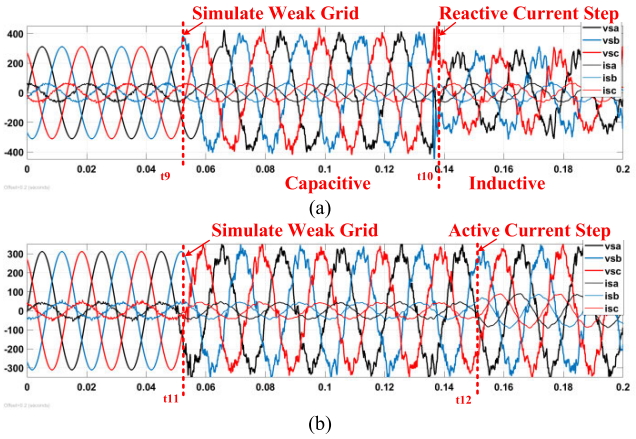

FIGURE 6. PCC voltages and currents waveforms in weak grid simulation. (a) In reactive current step. (b) In active current step.

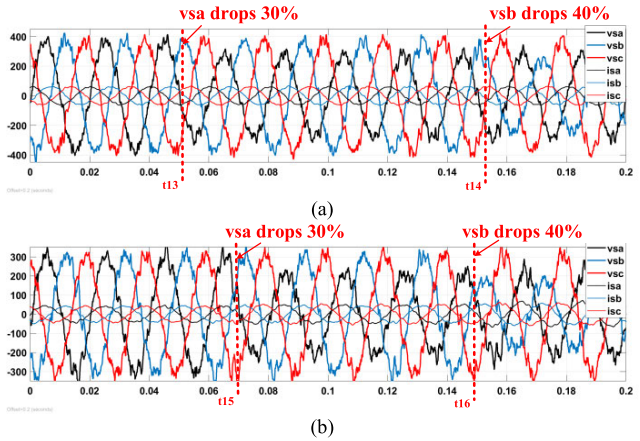

FIGURE 7. PCC voltages and currents waveforms in unbalanced weak grid simulation. (a) In reactive power state. (b) In active power state.

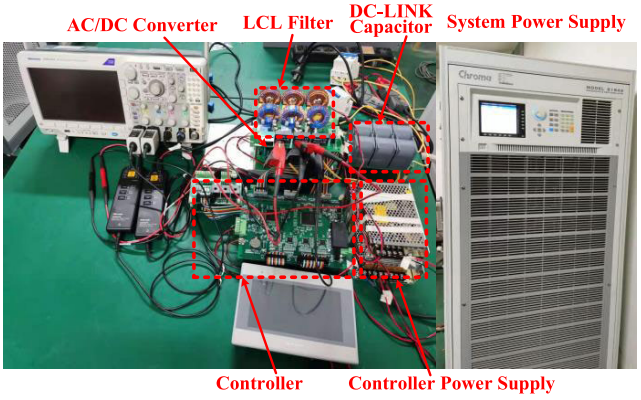

FIGURE 8. The downsized LCL prototype.

C. UNBALANCED WEAK GRID SIMULATION

In Fig. 7(a), the power sources are balanced weak grid at the first, and the converter outputs -20A reactive current. At the time t_{13} and t_{14}, v_{sa} and v_{sb} drop by 30% and 40%, respectively, the currents are still sinusoidal balanced waves with same amplitude all the time in unbalanced weak grid condition. In Fig. 7(b), the power sources are balanced weak grid at the first, and the converter's load is 100Ω resistor. Similarly, at the time t_{15} and t_{16}, v_{sa} and v_{sb} drop by 30% and 40%, respectively, the currents are still sinusoidal balanced waves with same amplitude all the time in unbalanced weak grid condition.

Through the simulations, we can conclude that in whatever strong grid, weak grid or unbalanced weak grid, in whatever active or reactive power state, the improved three-stages PBC can stabilize the system, response to control command rapidly, and the currents are balanced sinusoidal waves all the time.

VI. EXPERIMENTAL VERIFICATION

To further verify the effectiveness of the improved three-stages cascading PBC strategy, a downsized grid-connected LCL converter prototype of 5kW is built, as shown in Fig.8,

TABLE 3. Main circuit parameters of prototype.

Parameters	Value
Rated AC voltage (V)	190
Rated DC voltage (V)	400
Grid-side filter induct. L_1 (mH)	0.250
Converter-side filter induct. L_2 (mH)	1.000
Filter capacitor C (μF)	4.4
Filter series resistor R_1 (Ω)	0.1
Converter series resistor R_2 (Ω)	0.2
Filter parallel admittance G_f (1/Ω)	0.0002
DC-link capacitor (μF)	300
Switching frequency (kHz)	12.8

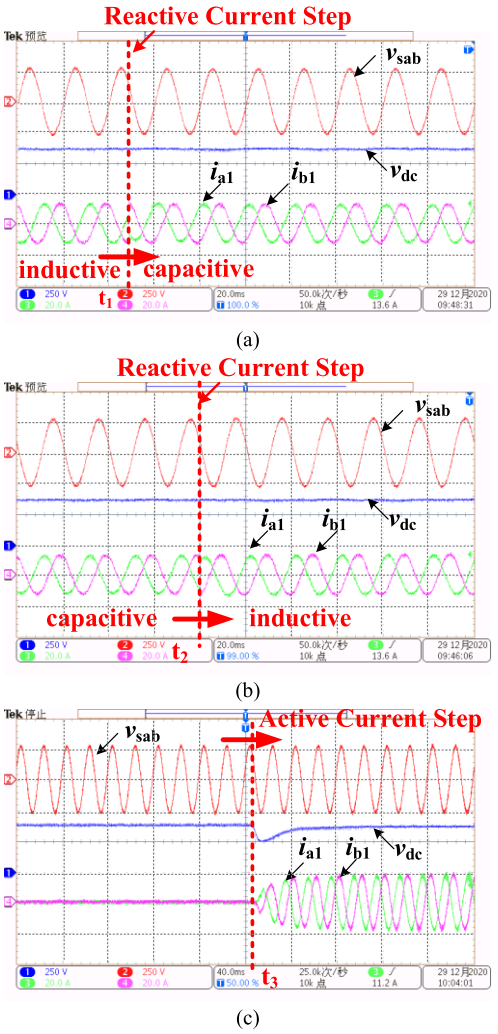

FIGURE 9. PCC voltage, currents and DC voltage waveforms in strong grid experiment. (a) From inductive to capacitive current step. (b) From capacitive to inductive current step. (c) Active current step.

and various experiments are also conducted in the prototype. The main circuit parameters are shown in Table 3, and the control coefficients are shown in Table 4.

A. STRONG GRID EXPERIMENT

In the experiment, the strong grid is supplied by Chroma 61845 power supply. In Fig. 9(a) and (b), the converter

TABLE 4. Control coefficients of prototype.

Coefficients	Value
DC voltage control kp	0.05
DC voltage control ki	5.0
Damping coefficient r_{11}	20
Damping coefficient r_{22}	10.0
Damping coefficient g_{33}	0.020

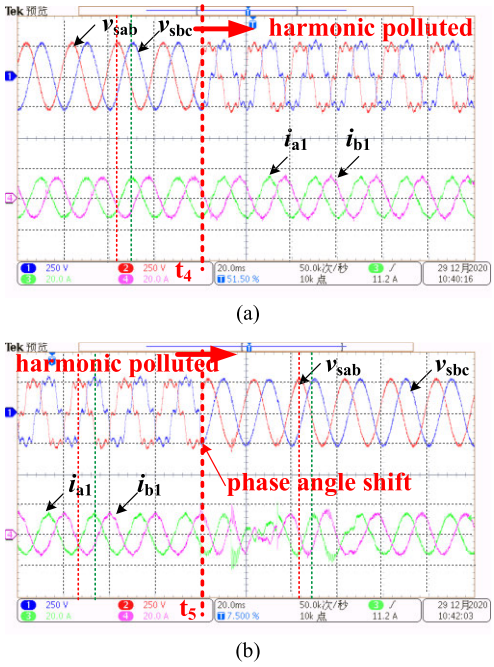

FIGURE 10. PCC voltages and currents waveforms in weak grid experiment. (a) From strong to weak grid condition. (b) From weak to strong grid condition.

outputs −10A inductive current at the first. At the time t_1 and t_2, the current reference is set as 10A (capacitive) and -10A (inductive), respectively, the converter tracks the reference current step quickly, and the DC voltage has no obvious fluctuation. In Fig. 9(c), the converter DC voltage stays at 400V. At the time t_3, a 50Ω resistor is put in the DC capacitor. Then, the DC voltage drops about 120V, and it recovers quickly to the reference voltage again after 20ms transient process. The converter currents track the active current reference step rapidly, and its response time is less than 20ms. The currents' THD is 3.46% in the strong grid experiment process.

B. WEAK GRID EXPERIMENT

In the experiment, the weak grid is supplied by 110V fundamental voltage with 5.5V 3rd harmonic, 11V 5th harmonic and 16.5V 7th harmonic voltages. In Fig. 10, the power sources are perfect sinusoidal waves at the first, and the converter outputs 10A reactive current. At the time t_4, the 3rd, 5th and 7th harmonics are set as 5.5V, 11V and 16.5V, respectively.

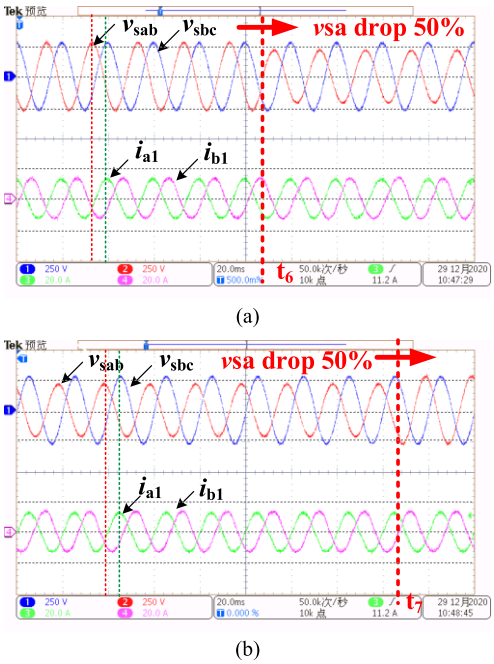

FIGURE 11. PCC voltages and currents waveforms in unbalanced grid experiment. (a) From balanced to unbalanced grid condition. (b) From unbalanced to balanced grid condition.

As a result, the PCC voltages deteriorate with THD of 18.7%. However, the currents are still sinusoidal balanced waves with same amplitude, and the currents' THD is 4.23%. At the time t_5, the 3rd, 5th and 7th harmonics are all reset as 0V, the PCC voltages restore to perfect sinusoidal waves, and the currents are still perfect sinusoidal balanced waves with same amplitude. Because there is a phase shift at the time t_4, the currents return to normal waveform after a transient process.

C. UNBALANCED GRID EXPERIMENT

In Fig. 11, the power sources are balanced grid at the first, and the converter outputs 10A reactive current. At the time t_6, v_{sa} drops by 50%, and the currents are still perfect sinusoidal balanced waves with same amplitude. At the time t_7, v_{sa} restores to the normal voltage, and the currents are still perfect sinusoidal balanced waves of same amplitude in the whole process.

Through the experiment, we can also conclude that in whatever strong grid, weak grid or unbalanced grid, in whatever active or reactive power state, the improved three-stages cascading PBC strategy can track the reference current rapidly with sinusoidal and balanced waves.

VII. CONCLUSION

In this paper, an improved three-stages cascading PBC strategy of a grid-connected LCL converter is proposed, and theory analysis, controller design, SIMULINK simulation and prototype experiment are studied respectively. The simulations and prototype experiments in strong grid, weak

grid and unbalanced grid are carried out respectively, and the results show that the converter currents are balanced sinusoidal waves all the time with good static and dynamic characteristics. Compared with traditional PBC, the improved three-stages cascading PBC has the advantages of easy implementation because of state variables decomposition and cascading control.

REFERENCES

[1] C. Bao, X. Ruan, X. Wang, W. Li, D. Pan, and K. Weng, "Step-by-step controller design for LCL-type grid-connected inverter with capacitor–current-feedback active-damping," *IEEE Trans. Power Electron.*, vol. 29, no. 3, pp. 1239–1253, Mar. 2014.

[2] F. Blaabjerg, R. Teodorescu, M. Liserre, and A. V. Timbus, "Overview of control and grid synchronization for distributed power generation systems," *IEEE Trans. Ind. Electron.*, vol. 53, no. 5, pp. 1398–1409, Oct. 2006.

[3] R. N. Beres, X. Wang, M. Liserre, F. Blaabjerg, and C. L. Bak, "A review of passive power filters for three-phase grid-connected voltage-source converters," *IEEE J. Emerg. Sel. Topics Power Electron.*, vol. 4, no. 1, pp. 54–69, Mar. 2016.

[4] R. Beres, X. Wang, F. Blaabjerg, C. L. Bak, and M. Liserre, "A review of passive filters for grid-connected voltage source converters," in *Proc. IEEE Appl. Power Electron. Conf. Expo.*, Mar. 2014, pp. 2208–2215.

[5] M. Liserre, F. Blaabjerg, and S. Hansen, "Design and control of an LCL-filter-based three-phase active rectifier," *IEEE Trans. Ind. Appl.*, vol. 41, no. 5, pp. 1281–1291, Sep./Oct. 2005.

[6] H. Karshenas and H. Saghafi, "Basic criteria in designing LCL filters for grid connected converters," in *Proc. IEEE Int. Symp. Ind. Electron.*, Jul. 2006, pp. 1996–2000.

[7] S. Sang, N. Gao, X. Cai, and R. Li, "A novel power-voltage control strategy for the grid-tied inverter to raise the rated power injection level in a weak grid," *IEEE J. Emerg. Sel. Topics Power Electron.*, vol. 6, no. 1, pp. 219–232, Mar. 2018.

[8] A. von Jouanne and B. Banerjee, "Assessment of voltage unbalance," *IEEE Trans. Power Del.*, vol. 16, no. 4, pp. 782–790, Oct. 2001.

[9] C. Yoon, X. Wang, F. M. Faria da Silva, C. L. Bak, and F. Blaabjerg, "Harmonic stability assessment for multi-paralleled, grid-connected inverters," in *Proc. Int. Power Electron. Appl. Conf. Expo.*, Nov. 2014, pp. 1098–1103.

[10] X. Wang, F. Blaabjerg, and P. C. Loh, "Proportional derivative based stabilizing control of paralleled grid converters with cables in renewable power plants," in *Proc. Energy Convers. Cong. Expo.*, 2014, pp. 4917–4924.

[11] R. Pena-Alzola, M. Liserre, F. Blaabjerg, M. Ordonez, and Y. Yang, "LCL-filter design for robust active damping in grid-connected converters," *IEEE Trans. Ind. Informat.*, vol. 10, no. 4, pp. 2192–2203, Nov. 2014.

[12] J. Roldan-Perez, E. J. Bueno, R. Pena-Alzola, and A. Rodriguez-Cabero, "All-pass-filter-based active damping for VSCs with LCL filters connected to weak grids," *IEEE Trans. Power Electron.*, vol. 33, no. 11, pp. 9890–9901, Nov. 2018.

[13] P. Cortes, M. P. Kazmierkowski, R. M. Kennel, D. E. Quevedo, and J. Rodriguez, "Predictive control in power electronics and drives," *IEEE Trans. Ind. Electron.*, vol. 55, no. 12, pp. 4312–4324, Dec. 2008.

[14] P. Lin, C. Zhang, P. Wang, X. Li, J. Xiao, P. Tu, and C. F. Hoong, "A global robust output regulation method for grid-connected inverter with LCL filter in weak grid condition," in *Proc. 12th IEEE Conf. Ind. Electron. Appl. (ICIEA)*, Jun. 2017, pp. 1646–1651.

[15] J. Xu, Q. Qian, and S. Xie, "Adaptive control method for enhancing the stability of grid-connected inverters under very weak grid condition," *Proc. Appl. Power Electron. Conf. Expo. (APEC)*, 2018, pp. 1141–1146.

[16] X. Chang, C. Lv, Q. Wang, W. Qin, M. Zhang, Y. Liu, and R. Fan, "Robust voltage resonance feedforward control strategy for LCL-type grid-connected inverters under weak grid condition," in *Proc. Asian Conf. Energy, Power Transp. Electrific. (ACEPT)*, Oct. 2018, pp. 1–6.

[17] D. Zhu, S. Zhou, X. Zou, Y. Kang, and K. Zou, "Phase-locked loop small-signal disturbance compensation control for three-phase LCL-type grid-connected converter under weak grid," in *Proc. Energy Conv. Congr. Expo. (ECCE)*, 2018, pp. 3108–3112.

[18] T. Liu, X. Hao, X. Yang, M. Zhao, and L. Xiong, "A novel grid voltage feed forward control strategy for three-phase grid-connected VSI with LCCL filter," *Proc. Intl. Sympo. Ind. Electron.*, May 2012, pp. 86–91.

[19] A. F. Cupertino, L. P. Carlette, F. Perez, J. T. Resende, S. I. Seleme, and H. A. Pereira, "Use of control based on passivity to mitigate the harmonic distortion level of inverters," in *Proc. IEEE PES Conf. Innov. Smart Grid Technol. (ISGT Latin America)*, Apr. 2013, pp. 1–7.

[20] D. Biel and J. M. A. Scherpen, "Passivity-based control of active and reactive power in single-phase PV inverters," in *Proc. Int. Symp. Ind. Electron. (ISIE)*, Edinburgh, Scotland, Jun. 2017, pp. 999–1004.

[21] J. Li, X. Lv, B. Zhao, Y. Zhang, Q. Zhang, and J. Wang, "Research on passivity based control strategy of power conversion system used in the energy storage system," *IET Power Electron.*, vol. 12, no. 3, pp. 392–399, Mar. 2019.

[22] J. Li, M. Wang, Y. Zhao, J. Wang, D. Yang, and X. Lv, "Passivity-based control of the hybrid rectifier for medium and high-power application," *IET Power Electron.*, vol. 12, no. 15, pp. 4070–4078, Dec. 2019.

[23] F. Yuanpeng, W. Jiuhe, and L. Jianguo, "Control strategy of Vienna rectifier with LCL filter under weak grid conditions," *Power Gener. Technol.*, vol. 40, no. 3, pp. 286–293, 2019.

[24] G. Liu, W. Wang, W. Wang, and K. Zhu, "Power feedforward method for passivity-based gridconnected PV inverter in weak grids," in *Proc. IEEE 4th Southern Power Electron. Conf. (SPEC)*, Dec. 2018, pp. 1–6.

[25] Y. Gui, W. Kim, and C. C. Chung, "Passivity-based control with nonlinear damping for type 2 STATCOM systems," *IEEE Trans. Power Syst.*, vol. 31, no. 4, pp. 2824–2833, Jul. 2016.

[26] Y. Jiang, C. Qin, X. Xing, X. Li, and C. Zhang, "A hybrid passivity-based control strategy for three-level T-type inverter in LVRT operation," *IEEE J. Emerg. Sel. Topics Power Electron.*, vol. 8, no. 4, pp. 4009–4024, Dec. 2020.

[27] J. Zhao, W. Wu, N. Gao, H. Wang, H. S. Chung, and F. Blaabjerg, "Combining passivity-based control with active damping to improve stability of LCL filtered grid-connected voltage source inverter," in *Proc. IEEE Int. Power Elec App Conf. Expo. (PEAC)*, Shenzhen, China, Nov. 2018, pp. 1–6.

JIANGUO LI (Member, IEEE) was born in Hebei, China, in 1975. He received the B.S. degree from the Department of Electrical Engineering (DEE), North China Electric Power University (NCEPU), Baoding, China, in 1997, the M.S. degree from the DEE, Tsinghua University, Beijing, China, in 2005, and the Ph.D. degree from the DEE, NCEPU, Beijing, in 2017. He is currently an Associate Professor with the College of Automation, Beijing Information Science and Technology University. His current research interests include bidirectional dc-dc converter, high-frequency-link power conversion systems, and flexible ac and dc transmission or distribution systems.

YAJING ZHANG (Member, IEEE) was born in Hebei, China, in 1984. She received the B.S. and Ph.D. degrees in electrical engineering from Beijing Jiaotong University, China, in 2008 and 2015, respectively. From February 2015 to August 2017, she was a Postdoctoral Researcher in control science and engineering with the Beijing University of Chemical Technology, China. Since 2017, she has been a Lecturer with the College of Automation, Beijing Information and Science Technology University, Beijing, China. Her current research interests include high-efficiency dc-dc converters, high-power density dc-dc converters, and renewable energy applications.

YUMING ZHAO was born in Jilin, China, in 1978. He received the B.S. and Ph.D. degrees from the Department of Electrical Engineering, Tsinghua University, Beijing, China, in 2001 and 2006, respectively. He is currently a Senior Engineer (Professor Level) with Shenzhen Power Supply Company Ltd., Shenzhen, China. His main research interest includes dc distribution power grid.

JIUHE WANG was born in Jilin, China. He received the B.E. degree in electrical engineering from the School of Electrical and Control Engineering, Liaoning Technical University, Fuxin, China, in 1982, and the Ph.D. degree in control science and engineering from the School of Information Engineering, University of Science and Technology Beijing, Beijing, China, in 2005. He is currently a Professor with the School of Automation, Beijing Information Science and Technology University, Beijing. His research interests include nonlinear control of power electronic converter, power quality control, and microgrid.

LI REN was born in Shanxi, China, in 1982. He received the Ph.D. degree in electrical engineering from Tsinghua University, Beijing, China, in 2014. He is currently a Research and Development Engineer with the Tianjin Research Institute for Advanced Equipment, Tsinghua University. His main research interests include operation, control, and protection of power systems, and power electronics.

YUFAN LIU was born in Shandong, China, in 1996. He received the B.S. degree from Beijing Information Science and Technology University, Beijing, China, in 2019, where he is currently pursuing the M.S. degree with the College of Automation. His current research interest includes bidirectional dc-dc converter.